TRANSITION METAL OXIDES AS PASSIVATED HOLE-CONTACTS LAYER FOR SILICON SOLAR CELLS: INTRINSIC AND EXTRINSIC DEFECTS IN MoO_3 FROM FIRST-PRINCIPLES CALCULATIONS

Md. Anower Hossain[1,2*], Sergey Rashkeev[1], Vinod Madhavan[1], Tian Zhang[2], Chang-Yeh Lee[2], Bram Hoex[2], Nouar Tabet[1], and Amir Abdallah[1]
[1]Qatar Environment and Energy Research Institute, Hamad Bin Khalifa University, Doha 34110, Qatar
[2]School of Photovoltaic and Renewable Energy Engineering, UNSW Sydney, Sydney 2052, Australia
*Corresponding author: Md. Anower Hossain, Phone: +61 (0)468450858, e-mail: a.hossain@unsw.edu.au

ABSTRACT: In this work, we present first-principles calculations for different defects in MoO_3 oxide which is considered as a hole-selective contact for crystalline silicon solar cells. An attempt was made to understand the role of different defects in charge carrier transport. In particular, we consider intrinsic defects including oxygen vacancies (V_O) and molybdenum vacancies (V_{Mo}) as well as extrinsic defects (dopants) in MoO_3, namely, hydrogen (H), nitrogen (N), and silicon (Si). We show that some dopants have a shallow level in the MoO_3 bandgap close to the conduction band minimum (CBM) which could positively affect hole collection from silicon. The methodology used in this work should facilitate rational design of materials and processes for the charge carrier selective contacts for silicon solar cells.

Keywords: Transition metal oxides, Semiconductors, Defects, c-Si, Silicon solar cells, Doping, Passivation, Density functional theory, Modelling, Projected density of states, Charge carrier recombination

1 INTRODUCTION

The passivated emitter and rear contact (PERC) solar cell technology with its current record efficiency close to 25% on monocrystalline silicon, is predicted to dominate silicon solar cell technologies for mass production in the next decade.[1] It is generally expected that the efficiency of PERC silicon solar cells manufactured in high volume can go up to 25%.[2] To further improve the efficiency, silicon solar cells with so-called carrier-selective contacts are required. Currently, doped amorphous and poly-silicon contacts are the most mature carrier selective contacts that enabled silicon solar cells to reach efficiencies above 26%.[3, 4] An alternative approach is to use undoped transition metal oxides such as molybdenum trioxide (MoO_3), tungsten oxide (WO_3), and nickel oxide (NiO_x) as hole-selective contacts, which is particularly appealing as these layers show a significantly lower optical absorption compared to their doped silicon-based counterparts.[5-13]

MoO_3 is an emerging material which has shown its potential as hole-selective layer in silicon solar cells.[11-13] It has fascinating electrical, optical and band energetic properties that are known to be crucial for passivating hole-contact of silicon solar cells and for interfacial hole transporting layer of perovskite solar cells. Because of its high transparency in the visible part of the solar spectrum due to its relatively high bandgap of 3.2 eV,[14, 15] and its large work function of about 6 eV, MoO_3 was also used as a transparent contact in solar cells and organic electronics.[12]

As the electronic properties of semiconductors strongly depend on the presence of point defects, many of their electronic structure properties can be tuned by incorporating corresponding intrinsic defects and extrinsic dopants. While deep level defects act as minority charge carrier recombination centers and suppress the quantum efficiency of solar cells, incorporation of certain defects, especially in the carrier-collecting region, can assist the transport of majority carriers and reduce the concentration of minority carriers by suppressing the recombination in the carrier-collecting region.[16, 17] Therefore, defects with energy levels positioned in the region of carrier collection, *i.e.*, near the valence and conduction band edges of the interface between the contact material and Si could improve the performance of carrier selective contacts.

In this work, we tried to understand how different defects modify the electronic properties MoO_3. In particular, we considered intrinsic defects including oxygen vacancies (V_O) and molybdenum vacancies (V_{Mo}). The oxygen vacancy states are known as *n*-type defects for MoO_x ($x < 3$). It was shown that due to the high MoO_3 workfunction, the band alignment with silicon results in holes accumulating in silicon near the c-Si and molybdenum oxide interface and some defects in MoO_x film may facilitate hole transit through defect derived states. In particular, it was shown that dopant-free, substoichiometric molybdenum trioxide (MoO_x, $x < 3$) could be a hole-selective contact for silicon solar cells.[10]

In this work, we performed first-principles, density functional theory (DFT) based electronic structure calculations for a number of intrinsic defects (vacancies) as well as for extrinsic defects (dopants) including hydrogen (H), nitrogen (N), and silicon (Si) in MoO_3 and showed that both vacancies and dopants can positively affect the electronic properties of the material. Introduction of these defects typically occurs in the material fabrication process and depends on temperature, pressure, deposition environment, *etc*. These parameters may significantly affect the physical properties of the synthesized MoO_3 material. We calculated the defect formation energies and the defect level energies for the charged defects with respect to the MoO_3 bandgap. The defect level energies were found to significantly vary for different dopants which could provide a possibility to design MoO_3 contacts for solar cells with optimal transport properties.

2 COMPUTATIONAL DETAILS

The first-principles calculations were conducted using DFT based with projector augmented wave (PAW)[18] pseudopotentials as implemented in the Vienna Ab-initio Simulation Package (VASP).[19] The Perdew-Burke-Ernzerhof (PBE)[20] exchange-correlation density functionals as well as the Mo_pv ($4p^6 5s^1 4d^5$) and O

($2s^22p^4$) pseudopotentials were used in the calculations. Apart from the generalised gradient approximation (GGA) density functionals, the (GGA+U) methodology known as Dudarev's approach[21] (with U = 4.2 eV) was employed to take the on-site electronic correlations for localised d-orbitals of the transition metal atoms into account. A bulk 3×1×3 supercell of MoO_3 containing 36 formula units (144 atoms) was utilized in this study. A large supercell was considered to reduce errors related to finite size effects as described in Ref.[22] A plane wave basis set with a 520 eV energy cut-off was used to construct the electronic wavefunctions. The supercell was fully relaxed until the residual forces acting on all atoms became less than 0.01 Å eV^{-1}. The Brillouin zone was sampled using the Monkhorst-Pack scheme.[23] Van der Waals interactions between neighbouring MoO_3 bilayers were incorporated by the D3 method of Grimme which was reported to be successful in addressing structural and electronic properties.[24] The electronic density of states (DOS) was computed using a tetrahedron scheme; all performed calculations were spin-polarised.

Defect formation energy calculations provide useful information on defect stability as well as on thermodynamic transition levels between different charge states. The defect energy levels indicate whether a particular defect is a shallow donor/acceptor or deep defect. As the formation of a charged defect can be viewed as an exchange of electrons between the host atoms and the electronic reservoir, the formation energy of the defect (D) depends on the electronic Fermi energy (μ_e) and charge (q) as follows:[15, 25-27]

$$E^f(D,q) = E_{tot}^D(q) - E_{tot}^{bulk} + \sum n_i\mu_i + q(E_{VBM} + \mu_e) + \Delta^q \quad (1)$$

where $E_{tot}^D(q)$ is the total energy of the supercell containing the defect, and E_{tot}^{bulk} is the energy of the perfect supercell; n_i and μ_i are the number of atoms of a species i removed from/added to the supercell, and the corresponding chemical potential of the atom, respectively; the last term is the energy correction applied for charged defects to counter the self-interaction across the periodic boundary conditions of finite supercells. The zero of the electronic Fermi energy (μ_e) corresponds to the valence band maximum (E_{VBM}) in the defect free perfect supercell; the μ_e values are varied from 0 to the band gap energy (3.2 eV) in MoO_3. The corrections related to band alignments, and interactions among the charged defects originated from periodic boundary condition of supercell, were also conducted.[25, 28] It was previously reported by Lambert *et al.*[26] that for MoO_3, the chemical potential of Mo atom should be calculated using the BCC-Mo crystal, while the chemical potential of oxygen gas molecule should be calculated considering the standard formation energy of MoO_3:

$$\Delta G_f^{MoO_3}(p_{O_2}^0, T^0) = \mu_{MoO_3(s)} - \mu_{Mo(s)} - \frac{3}{2}\mu_{O_2(g)}(p_{O_2}^0, T^0) \quad (2)$$

where $\Delta G_f^{MoO_3}(p_{O_2}^0, T^0)$ and $\mu_{O_2(g)}(p_{O_2}^0, T^0)$ are the formation energy of MoO_3 and chemical potential of oxygen at standard condition. Because of its gaseous state, the chemical potential of oxygen strongly depends on pressure and temperature. However, the chemical potential of MoO_3 ($\mu_{MoO_3(s)}$) and Mo ($\mu_{Mo(s)}$) does not strongly depend on the partial pressure and temperature due to their solid nature. Therefore, the chemical potential of oxygen gas at room temperature was determined using the ideal gas law as follows:

$$\mu_{O_2(g)}(p_{O_2}, T) = \mu_{O_2(g)}(p_{O_2}^0, T^0) + \frac{1}{2} k_B T \log\left(\frac{p_{O_2}}{p_{O_2}^0}\right) \quad (3)$$

An assumption that the chemical potential of oxygen in MoO_3 is equal to that of oxygen gas corresponds to the case of O-rich conditions.

3 RESULTS AND DISCUSSIONS

3.1 Intrinsic defects: oxygen and molybdenum vacancies in MoO_3

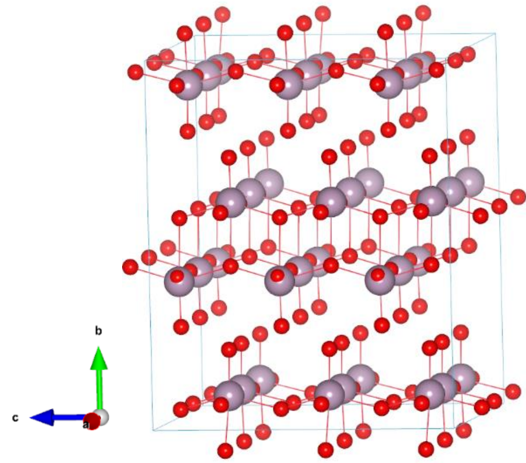

Figure 1. A schematic of fully relaxed 3×1×3 supercell of orthorhombic α-MoO_3 structure. Mo and O atoms are shown by purple and red spheres, respectively.

As shown in Figure 1, the layered α-MoO_3 is comprised of weak Van der Waals bonded layers of edge-sharing Mo−O_6 octahedra. The three types of symmetry-equivalent oxygen atomic sites are: symmetric (O_s) sites which connect the Mo atoms to form chains in the *c*-direction, asymmetric (O_a) sites which connect two Mo atoms and are oriented along the *a*-direction, and terminal (O_t) sites which face interlayer spacing along *b*-direction. The formation energy vs. the Fermi level are plotted for the oxygen vacancy (V_O) at all three inequivalent oxygen sites, for the charge states q = 0, +1, and +2 (Figure 2). The oxide growth condition was assumed to be oxygen-rich, meaning that the removed oxygen atoms from the MoO_3 structure will form oxygen molecules in the ambient atmosphere. Among the multiple possible charge states of the point defect, the lowest formation energy corresponds to the most stable charge state for a given Fermi level. A similar approach should be used for oxygen-poor conditions.

The oxygen vacancy formation energies for the obtained neutral states were 3.86 eV, 2.0 eV, and 1.56 eV for the symmetric, asymmetric, and terminal sites, respectively, suggesting that vacancy formation process is favourable for the terminal sites rather than for two other sites. A transition of +2 state to +1 state followed by the transition from +1 to neutral state was observed for the oxygen vacancies when moving through the band gap. The transition energy of +2/+1 transition is the lowest for V_{Oa}

(0.24 eV above VBM, Figure 2b). These result qualitatively agrees with results obtained earlier in Ref.[26]

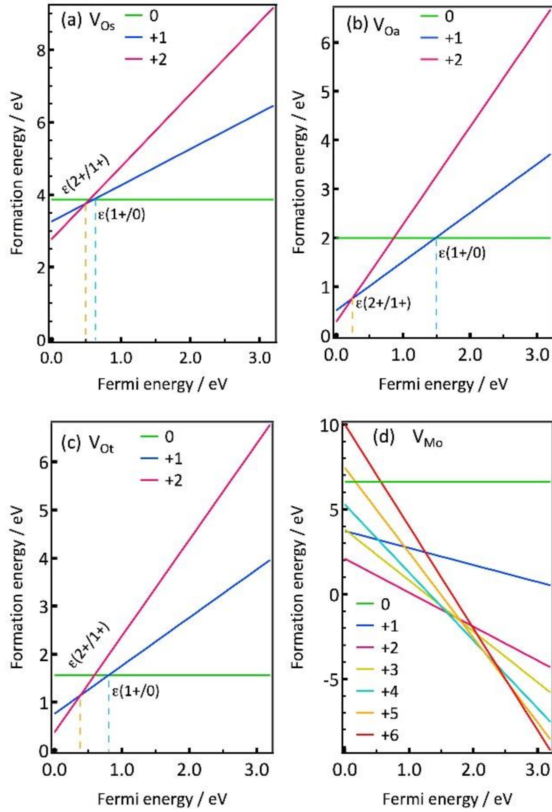

Figure 2. The vacancy formation energies at (a) O_s; (b) O_a, and (c) O_t sites of the MoO_3 supercells at charge states of $q = 0, +1$, and $+2$ at the O-rich condition. Figure (d) shows the formation energy of the Mo vacancies at different charge states and O-rich condition.

The projected density of states (PDOS) plots in Figure 3 (a) shows that the conduction band of MoO_3 is dominated by the Mo states. Also, the PDOS plots indicate the appearance of V_O defect states in the MoO_3 band gap [Figures 3(b,c,d)], suggesting that the electrons released from a corresponding oxygen vacancy after removing a neutral oxygen atom have a tendency to occupy empty Mo 4d orbitals positioned at the bottom of the conduction band. In particular, it is clear that oxygen vacancies created within the MoO_3 layer [at the symmetric (O_s) and asymmetric (O_a) sites] shows levels closer to the CBM (i.e., are more shallow) than vacancies formed at the transition (O_t) sites with deeper defect levels. This is understandable because removal of transition oxygen atom will inevitably form dangling bonds that typically are deep level defects. Also, this result concludes that charge carrier transport assisted by oxygen vacancy defects is anisotropic and will mainly occur within the layers.

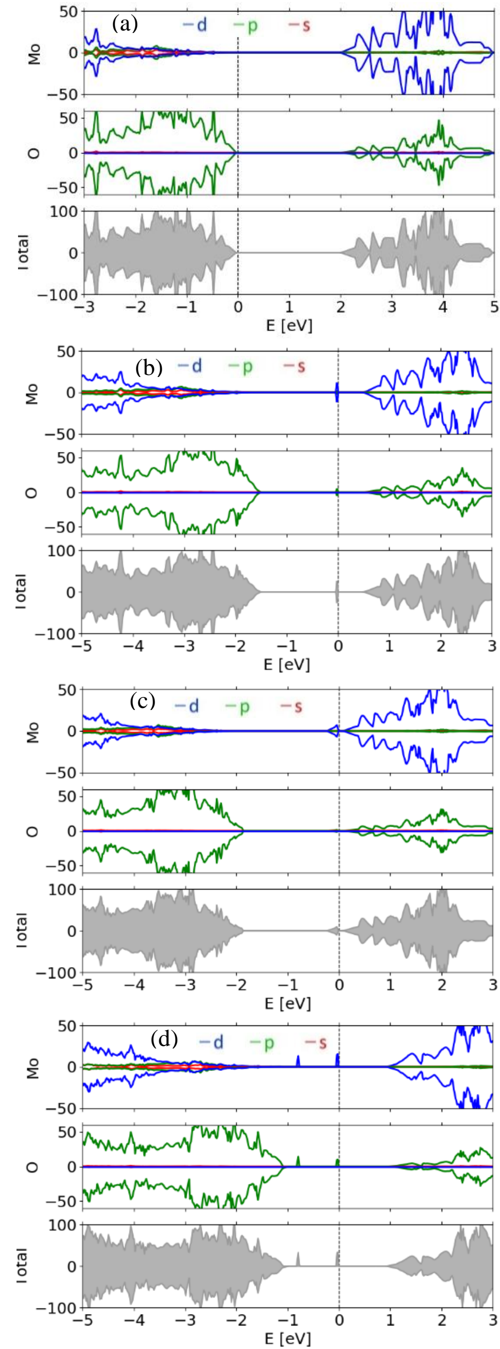

Figure 3. PDOS of: (a) pure MoO_3 supercell, (b) supercell with V_{Os} vacancy, (c) supercell with V_{Oa} vacancy, and (d) supercell with V_{Ot} vacancy. All vacancies are in their neutral charge state. The blue, green and red lines represent the d, p and s orbital contributions of corresponding atoms. The total DOS near the CBM is mainly composed of Mo 4d states, and the DOS near the VBM is mainly of O 2p states.

3.2 Extrinsic defects: substitutional Si(Mo), N(O), and interlayer H

Because of the observed high concentration of hydrogen in the as-deposited metal oxide by atomic layer deposition, we also considered hydrogen-induced defects as well as a few other extrinsic defects, such as Si(Mo) (silicon

substituting molybdenum) and N(O) (nitrogen substituting oxygen) in the MoO_3 matrix. Some selected results are shown in Figure 4.

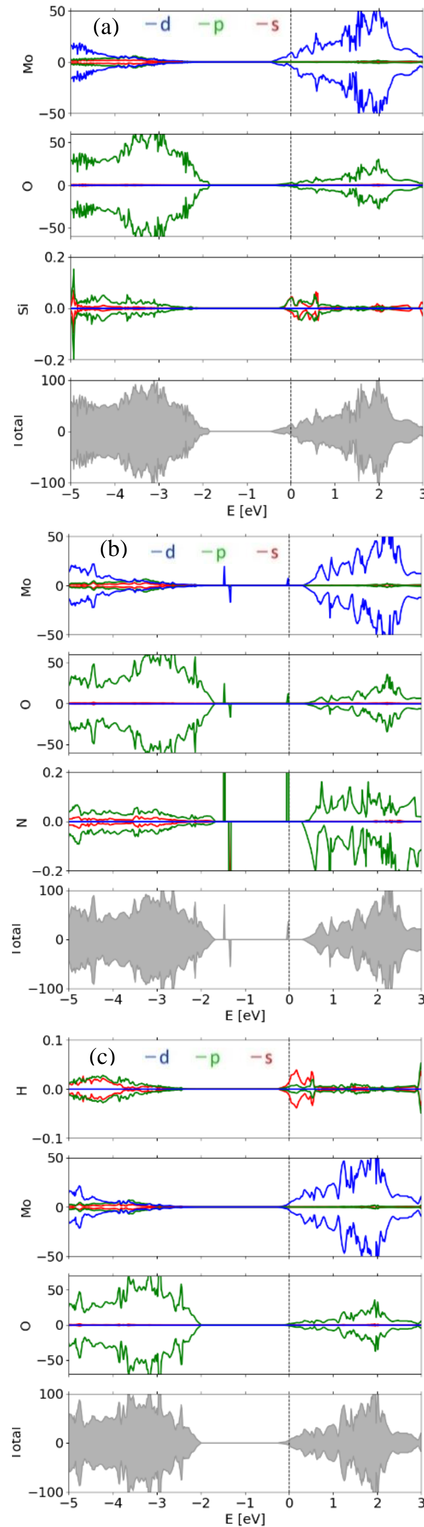

Figure 4. PDOS plots of the (a) Si (Mo), (b) N(O), and (c) interlayer H incorporated in the MoO_3 structure showing defect levels in the band gap. The blue, green and red colours represent the d, p and s orbital contributions of the respective elements, respectively.

The position of Fermi level for charge neutral defects indicates that Si(Mo) and interlayer H defects provide shallow levels positioned near the CBM in MoO_3 while N(O) levels are located deeper in the bandgap. It means that presence of nitrogen at the MoO_3 film fabrication stage may form deep dopant levels assisting carrier recombination in the device while the presence of hydrogen induced defects should not negatively affect the performance of solar cells containing MoO_3 passivating layer.

4 CONCLUSIONS

In summary, we considered the incorporation of different intrinsic and extrinsic defects in the MoO_3 which results in an appearance of defect levels within the band gap of the oxide. We suggest that some of these defects have shallow levels in the MoO_3 bandgap and, therefore, should suppress the recombination of charge carriers in the carrier-collecting region of the silicon solar cells thus increasing the solar energy conversion efficiency. Energy levels for other defects, however, are located deeper in the bandgap and may assist carrier recombination which is highly undesirable. The methodology used in this work should facilitate rational design of materials and processes for the charge carrier selective contacts in silicon solar cells.

5 ACKNOWLEDGEMENTS

This work was supported by a grant from the Qatar National Research Fund (a member of Qatar Foundation; Grant No. NPRP9-021-2-009).

6 REFERENCES

1. Green, M. A. *Sol. Energ. Mat. Sol. C.* **2015,** 143, 190-197.
2. Green, M. A.; Emery, K.; Hishikawa, Y.; Warta, W.; Dunlop, E. D.; Levi, D. H.; Ho-Baillie, A. W. Y. *PROG. PHOTOVOLTAICS* **2017,** 25, (1), 3-13.
3. Feldmann, F.; Bivour, M.; Reichel, C.; Hermle, M.; Glunz, S. W. *Sol. Energ. Mat. Sol. C* **2014,** 120, 270-274.
4. Yoshikawa, K.; Kawasaki, H.; Yoshida, W.; Irie, T.; Konishi, K.; Nakano, K.; Uto, T.; Adachi, D.; Kanematsu, M.; Uzu, H.; Yamamoto, K. *Nature Energy* **2017,** 2, 17032.
5. Melskens, J.; Loo, B. W. H. v. d.; Macco, B.; Black, L. E.; Smit, S.; Kessels, W. M. M. *IEEE Journal of Photovoltaics* **2018,** 8, (2), 373-388.
6. Zhang, T.; Lee, C.-Y.; Wan, Y.; Lim, S.; Hoex, B. *J. Appl. Phys.* **2018,** 124, (7), 073106.
7. Zhang, T.; Lee, C.-Y.; Gong, B.; Lim, S.; Wenham, S.; Hoex, B. *J. Vac. Sci. Technol. A* **2018,** 36, (3), 031601.
8. Chang-Yeh, L.; Mohammad Izzat Abdul, A.; Stuart, W.; Bram, H. *Jpn. J. Appl. Phys.* **2017,** 56, (8S2), 08MA08.
9. Hoex, B.; Dielen, M.; Lei, M.; Zhang, T.; Lee, C.-Y. *AIP Conf. Proc.* **2018,** 1999, (1), 040010.
10. Battaglia, C.; Nicolás, S. M. d.; Wolf, S. D.; Yin, X.; Zheng, M.; Ballif, C.; Javey, A. *Appl. Phys. Lett.* **2014,** 104, (11), 113902.

11. Battaglia, C.; Yin, X.; Zheng, M.; Sharp, I. D.; Chen, T.; McDonnell, S.; Azcatl, A.; Carraro, C.; Ma, B.; Maboudian, R.; Wallace, R. M.; Javey, A. *Nano Lett.* **2014,** 14, (2), 967-971.
12. Sacchetto, D.; Jeangros, Q.; Christmann, G.; Barraud, L.; Descoeudres, A.; Geissbühler, J.; Despeisse, M.; Hessler-Wyser, A.; Nicolay, S.; Ballif, C. *IEEE Journal of Photovoltaics* **2017,** 7, (6), 1584-1590.
13. Woojun, Y.; James, E. M.; Eunhwan, C.; David, S.; Nicole, A. K.; Erin, C.; Young-Woo, O.; Phillip, P. J.; Ajeet, R.; Robert, J. W. *Jpn. J. Appl. Phys.* **2017,** 56, (8S2), 08MB18.
14. Carcia, P. F.; McCarron, E. M. *Thin Solid Films* **1987,** 155, (1), 53-63.
15. Peelaers, H.; Chabinyc, M. L.; Van de Walle, C. G. *Chem. Mater.* **2017,** 29, (6), 2563-2567.
16. Richter, A.; Hermle, M.; Glunz, S. W. *IEEE Journal of Photovoltaics* **2013,** 3, (4), 1184-1191.
17. Liu, Y.; Stradins, P.; Deng, H.; Luo, J.; Wei, S.-H. *AIP Appl. Phys. Lett.* **2016,** 108, (2), 022101.
18. Blöchl, P. E. *Phys. Rev. B* **1994,** 50, (24), 17953-17979.
19. Kresse, G.; Joubert, D. *Phys. Rev. B* **1999,** 59, (3), 1758-1775.
20. Perdew, J. P.; Burke, K.; Ernzerhof, M. *Phys. Rev. Lett.* **1996,** 77, (18), 3865-3868.
21. Dudarev, S. L.; Botton, G. A.; Savrasov, S. Y.; Humphreys, C. J.; Sutton, A. P. *Phys. Rev. B* **1998,** 57, (3), 1505-1509.
22. Lany, S.; Zunger, A. *Phy. Rev. B* **2008,** 78, (23), 235104.
23. Monkhorst, H. J.; Pack, J. D. *Phys. Rev. B* **1976,** 13, (12), 5188-5192.
24. Grimme, S.; Antony, J.; Ehrlich, S.; Krieg, H. *J. Chem. Phys.* **2010,** 132, (15), 154104.
25. Walle, C. G. V. d.; Neugebauer, J.; E., P. W. *J. Appl. Phys.* **2004,** 95, (8), 3851-3879.
26. Lambert, D. S.; Murphy, S. T.; Lennon, A.; Burr, P. A. *RSC Advances* **2017,** 7, (85), 53810-53821.
27. Jiang, H.; Stewart, D. A. *ACS Appl. Mater. Interfaces* **2017,** 9, (19), 16296-16304.
28. Freysoldt, C.; Neugebauer, J.; Van de Walle, C. G. *Phys. Rev. Lett.* **2009,** 102, (1), 016402.